Development and characterization of an atmospheric pressure plasma reactor compatible with spatial ALD

Fadi Zoubian, Hervé Rabat, Olivier Aubry, Nicolas Dumuis, Sébastien Dozias, David Munoz-Rojas, Dunpin Hong

HAL Id: hal-02160263
https://hal.science/hal-02160263

Submitted on 19 Nov 2020

PAPER • OPEN ACCESS

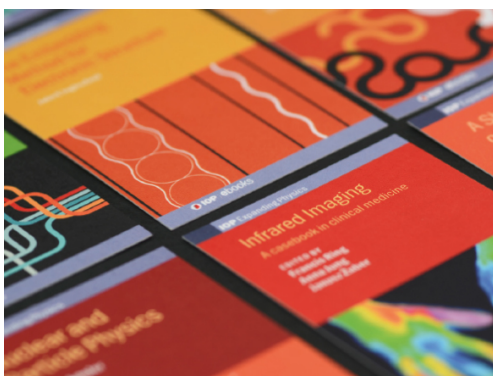# Development and characterization of an atmospheric pressure plasma reactor compatible with spatial ALD

To cite this article: F Zoubian *et al* 2019 *J. Phys.: Conf. Ser.* **1243** 012002

View the article online for updates and enhancements.

Recent citations

- Atmospheric Plasma-Enhanced Spatial Chemical Vapor Deposition of SiO2 using Trivinylmethoxysilane and Oxygen Plasma
Viet Huong Nguyen *et al*

Development and characterization of an atmospheric pressure plasma reactor compatible with spatial ALD

F ZOUBIAN¹*, H RABAT¹, O AUBRY¹, N DUMUIS¹, S DOZIAS¹, D MUÑOZ-ROJAS² and D HONG¹*

¹ GREMI UMR 7344 University of Orléans – CNRS, Orléans, 45000, France

² Univ. Grenoble Alpes, CNRS, Grenoble INP, LMGP, F-38000 Grenoble, France.

*Corresponding authors: fadi.zoubian@univ-orleans.fr and
dunpin.hong@univ-orleans.fr

Abstract. Dielectric Barrier Discharges (DBD) are widely used for atmospheric pressure plasma generation. The possibility of their adaptation in custom-made configurations makes them potential candidate to assist deposition processes. In fact, the increased need of high-quality thin films forces to improve the deposition techniques. New processes should be able to work in less constrained conditions such as atmospheric pressure rather than vacuum and to have faster deposition rates while respecting the same high quality of the deposited films. In this paper we present the development of a surface dielectric barrier discharge plasma reactor to assist an atmospheric spatial atomic layer deposition process. The reactor was fabricated with 3D printing and the plasma was generated by a surface dielectric barrier discharge powered by a microsecond pulsed high voltage power supply. The dissipated power was measured for different configurations, and thanks to the micro discharges imaging, it was observed that the thickness and the shape of the dielectric barrier influenced the micro discharges distribution on the dielectric surface. The plasma reactor exhaust gas was chemically analyzed by FTIR spectroscopy and micro gas chromatography. The ozone concentration was determined as function of frequency of the power supply.

1. Introduction

High quality thin films become the essential component in many technological applications such as photovoltaics and microelectronics. Atomic Layer Deposition (ALD) is a very reliable technique widely used to elaborate such films. The conventional ALD is based on a time sequenced injection of precursors and co-reactants to the deposition zone. It enables an accurate control of the film growth. However, it requires time for pumping before every sequence leading to slow deposition rates [1, 2]. Therefore, it is not compatible with most industrial needs. To meet the increasing demand on these films, elaboration processes should be improved to gain in performance and rentability without sacrificing the reliability and the quality of the deposited materials. Spatial Atomic Layer Deposition (SALD) is a variant of conventional ALD where the precursors and the co-reactants are separated in space rather than in time [3]. The major advantage of SALD is the possibility to work at atmospheric pressure. The elimination of pumping exhibits a considerable gain in time as well as in cost. Furthermore, an atmospheric plasma can be integrated to the SALD as source of reactive species, such as ozone, replacing the co-reactants [4], [5]. This process, so-called Plasma Enhanced Atmospheric Pressure SALD (PE-AP-SALD), permits more flexibility in processing conditions such as working at lower temperature (<200 °C). In addition it allows the use of larger choice of precursors therefore obtaining a wider range of material properties [6].

In this paper, we present an atmospheric plasma reactor designed to assist the SALD process. The reactor has been designed to be compatible with our SALD head [7], [8]. 3D printing was used to realize the reactor. The plasma was generated by a surface dielectric barrier discharge powered by a microsecond

pulsed High Voltage (HV) power supply. We investigated the effect of the thickness and the shape of the dielectric barrier on the distribution of micro discharges along the surface. We realized the electrical characterization and we measured the dissipated power by the DBD. And finally, we analyzed the plasma reactor exhaust gas and determined the concentration of generated ozone as function of discharge parameters.

2. Experimental setup

2.1. Plasma reactor

The plasma reactor is constituted by the reactor chamber, the DBD arrangement and the DBD support as shown in Figure 1. All parts were created with Autodesk Inventor® and printed with the Form 2 3D printer from Formlabs®. It is based on stereolithography (SLA) 3D printing using a 405 nm laser to cure solid isotropic parts with high resolution from a liquid photopolymer resin. The resin used in this work is the Clear Resin reference from Formlabs®, it supports a print resolution down to 25 microns. In addition, it presents good dielectric properties allowing it to be used as dielectric in the DBD arrangement. After printing, the parts are cleaned with isopropyl alcohol to wash liquid resin off the completed parts before the post-curing which provides the light and heat necessary for the materials to achieve their optimal properties.
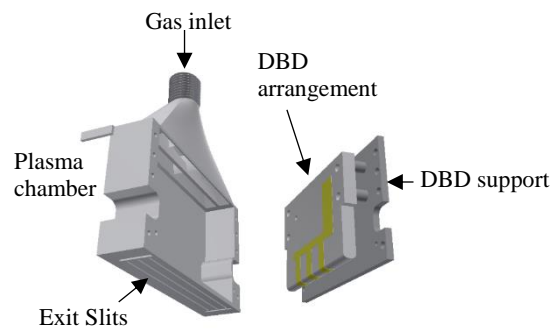

Figure 1. Schematic view of the plasma reactor with its components.

The DBD arrangement is formed with a 3D printed dielectric barrier including a cavity, as shown in Figure 2-a, allowing the introduction of an inox plate inside to form the inner (buried) electrode. The cavity was than filled with the liquid resin and treated with post-curing. The outer (exposed) electrode has a fork shape realized with copper tape.
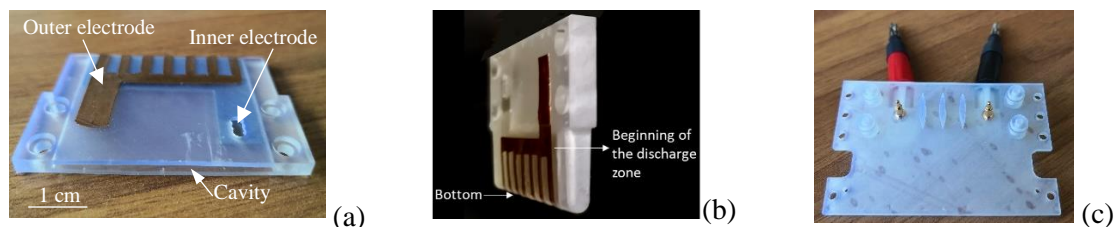
Figure 2. (a) The DBD arrangement showing the inner and outer electrodes and (b) a side view of the DBD. (c) The DBD support with the connections to the HV power supply.

Figure 2-b represents a side view of the DBD showing the evolution of the shape corresponding to the DBD2 illustrated in figure 4. The DBD support has for role to handle the DBD arrangement inside the reactor chamber and it consists a lid for the chamber. It is equipped with spring loaded contact

connectors ensuring the connection of the DBD arrangement to the High Voltage power supply as shown in Figure 2-c.

The reactor chamber has dimensions of 63x42x16 mm^3 enabling perfect assembly with our SALD head. The final configuration of the plasma reactor added to the SALD head is shown in **Figure 3**. The ensemble is to be placed at 50-200 µm from the moving substrate. The working gas is injected by the gas inlet. The precursors are injected through the SALD head while the plasma delivers reactive species resulting from the interaction between the working gas and the micro discharges to the deposition surface through exit slits. The generated reactive species can be categorized into two groups: long life species like ozone obtained when using oxygen or air as inlet gas, and short life species like H radicals (OH, H_2O, NH, ...) obtained with a mixture of gases (O_2, N_2O and/or NH_3, H_2…). The distance separating the plasma and the deposition surface must be as small as possible to enable the action of short-life reactive species on the sample surface.
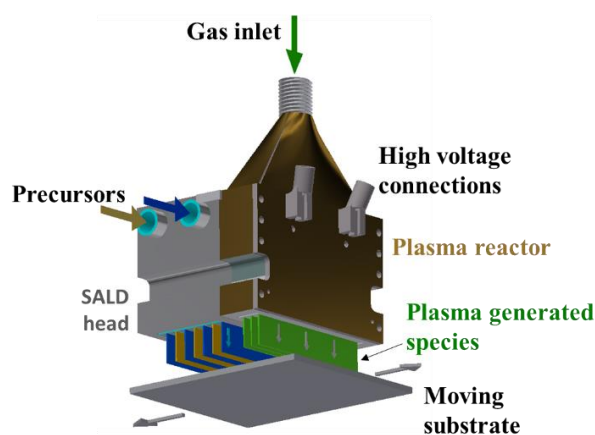

Figure 3. The plasma reactor (right part) added to the SALD head (left part).

Three different forms of dielectric barrier were realized as shown in Figure 4. DBD1 has a constant thickness of 2.2 mm. For DBD2 and DBD3, the thickness at the middle (beginning of the discharge zone) is 3.4 and 6.2 mm respectively. It decreases progressively to reach 2.2 mm at the bottom.
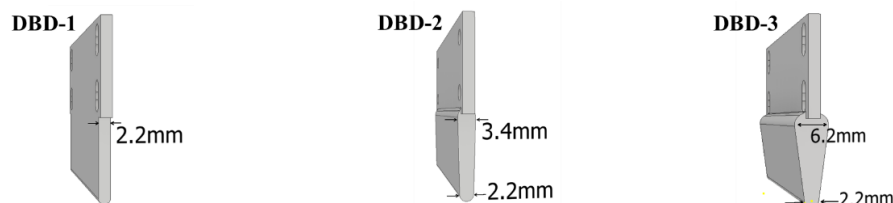

Figure 4. Schematic representation of the three dielectric barriers with different thickness.

2.2. Electrical setup

Figure 5-a shows a schematic representation of the setup for electrical supply and measurements. The inner electrode was grounded via a 2 nF capacitor allowing measurements of the discharge current integration. The DBD is powered by a High Voltage power supply delivering a pulsed signal (of width about 20 µs) with amplitude up to 25 kV and adjustable frequency between 1 and 10 kHz. The applied voltage was measured by a high voltage probe (Tektronix®, P60115A 1000X, 3.0 pF, 100 MΩ). A CT current transformer (Bergoz® CT-C1.0) was used for current measurements. Electrical signals were recorded by a LeCroy® WaveJet 354A oscilloscope with a bandwidth of 500 MHz and a sampling rate

of 2 Gs/s. The equivalent electrical circuit of the configuration is shown in figure 5-b. The voltage of the discharge is given by $v(t) = v_{HV} - v_C \approx v_{HV}$ since $v_{HV} \gg v_C$.
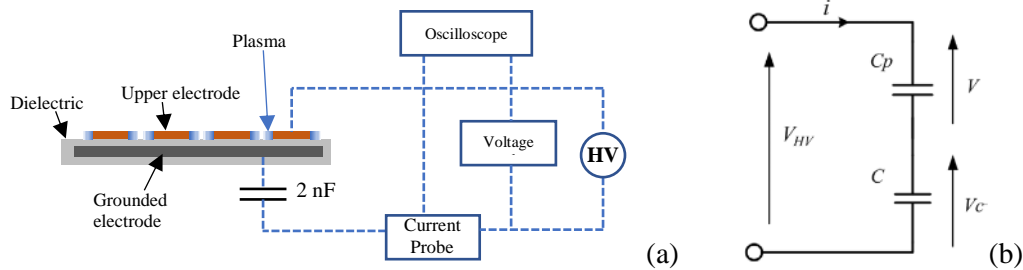

Figure 5. (a) Schematic configuration for electrical measurements, (b) the equivalent electrical circuit of the DBD configuration with the added capacitor C of 2 nF for the measurement of current integration.

An example of the measured current and voltage is shown in **Figure 6**-a. We can identify, on the current signal, the presence of current peaks related to the formation of filamentary micro discharges. These latter are formed when the applied voltage reaches a breakdown value. Other micro discharges are induced by the difference of potential between the charges accumulated on the dielectric surface and the outer electrode when the difference of potential reaches a threshold value.
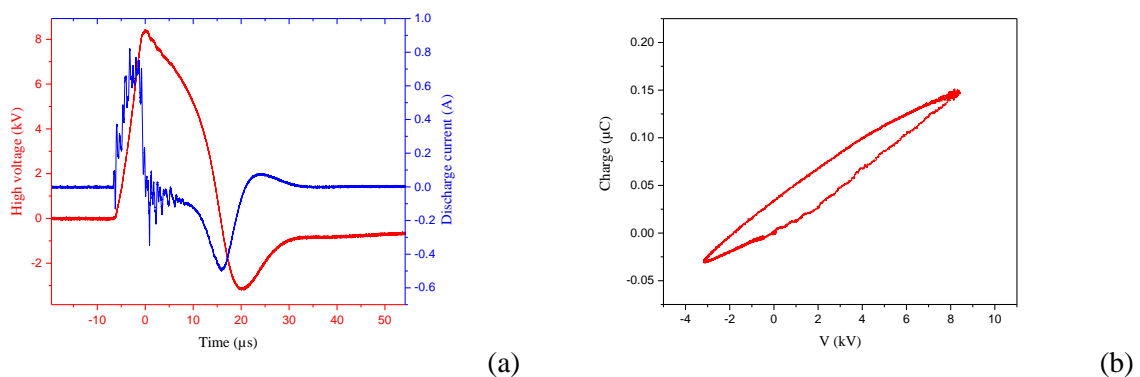

Figure 6. (a) Electrical signals showing the evolution of the high voltage and the current provided by the power supply which is the sum of displacement current and discharge current. (b) Example of the Lissajous figure used to calculate the dissipated power from the encircled area of Q-V curves.

The electrical configuration allows to measure the time-averaged power dissipated by the DBD *via* the so-called Lissajous Figure (**Figure 6**-b). It's achieved by drawing the curve of the charge of the inserted capacitor as function of the applied voltage for a full cycle. The encircled area of the curve gives the energy dissipated per cycle. The dissipated power is calculated by multiplying this value by the frequency:

$$P = f \int_0^T v \, dQ \qquad (1)$$

2.3. Micro discharges imaging

The distribution of micro discharge filaments on the surface of the dielectric barrier is captured using an iCCD istar 734 camera by Andor Technology®. The dielectric barrier was tilted with an angle of 30 degree in front of the camera lens as illustrated in **Figure 7**-a. This allows to have, at the same time, the view of the bottom and the back of the facing electrode as shown in **Figure 7**-b.
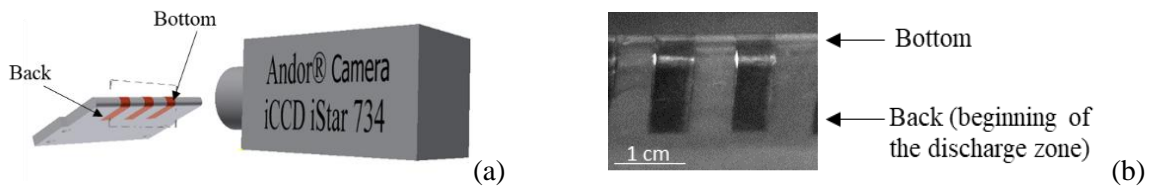
Figure 7. (a) schematic setup of the micro discharges imaging and (b) photograph of the electrode without discharge for reference.

2.4. Chemical investigation

The interactions between working gas and micro discharges are at the origin of reactive species generation. The exhaust gas was analyzed using the Fourier Transform Infra-Red spectroscopy (FTIR, thermo Scientific® Nicolet iS10). When the working gas is reconstituted air, O_2 is decomposed by electron impact. Oxygen atoms thus created recombine with dioxygen to form O_3 molecules. A prior calibration of the FTIR allows to measure the ozone concentration. Complementary analysis with micro gas chromatography, done with a Micro GC Fusion from INFICON® with measurement capability from 1 ppm to 100%, allows to monitor the presence of O_2 and CO_2 in the exhaust gas.

3. Results and discussion

3.1. Electrical measurements

Figure 8 shows the dissipated power for the three different DBDs configuration as function of the frequency. One can see first, that independently from the shape and the thickness of the barrier, the power increases linearly with the frequency. Same behavior was observed by Dong *et al*. with a variation of frequency between 0.5 and 5 kHz for two different kind of dielectric [9]. According to Portugal *et al.,* increasing the frequency from 8 to 20 kHz yields more micro discharges by unit time thus the power dissipation increases from 2 to 5 W approximately [10]]. While Pons *et al.* showed that increasing the thickness of the barrier by 50 % leads to a 40 % decrease in the dissipated power [[11]. This is consistent with our results showing 40 % less dissipated power when the thickness increases between DBD1 and DBD3.
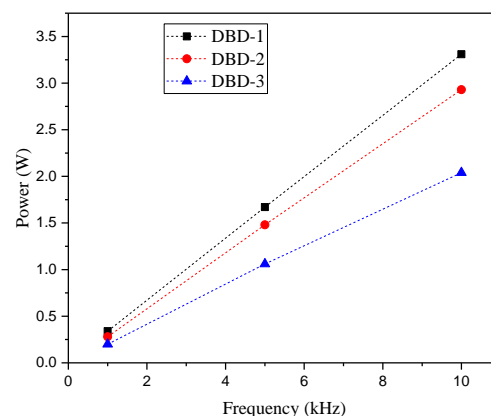

Figure 8. Dissipated power measured with Lissajous Figure as function of frequency for the three DBDs.

The measured discharge voltages of the three DBDs are given in Figure 9. As the barrier thickness increases, the voltage must increase to conserve an equivalent electric field for plasma production. As

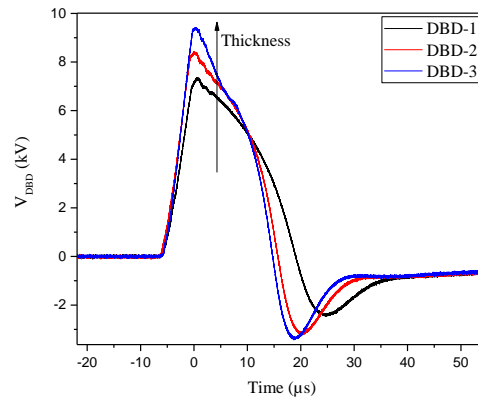presented below, the discharge voltage increases from 7.3 kV to 9.4 kV for DBD1 and DBD3 respectively.

Figure 9. The discharge voltages for the three DBDs.

3.2. Micro discharges imaging

To obtain a plasma closet to the deposition surface, the shape and the position of the DBD should be optimized. This starts with understanding the influence of the thickness and the shape of the dielectric barrier on the behavior of the discharge filaments. The three different DBDs represented in Figure 4 were studied. The DBDs were powered with a pulsed high voltage of 7.6 kV at a frequency of 5 kHz. The photographs taken with the experimental setup of Figure 7-a are presented in Figure 10. DBD1 shows a black region near the bottom of the dielectric caused by the absence of micro discharges in this zone. The barrier at this zone could be thicker, because the inox plate was manually prepared to have the same form as the bottom of the dielectric. This issue has less impact on the other DBDs. For DBD2 and 3, the evolutionary thickness allows a better distribution of the filaments at the bottom so that the plasma is present at the closet point from the reactor exit. However, DBD2 shows a homogenous distribution all over the electrodes contrary to DBD3 showing a black region in the back of the electrodes. This homogenous distribution prevents a potential overheating of the barrier at specific points risking its degradation.
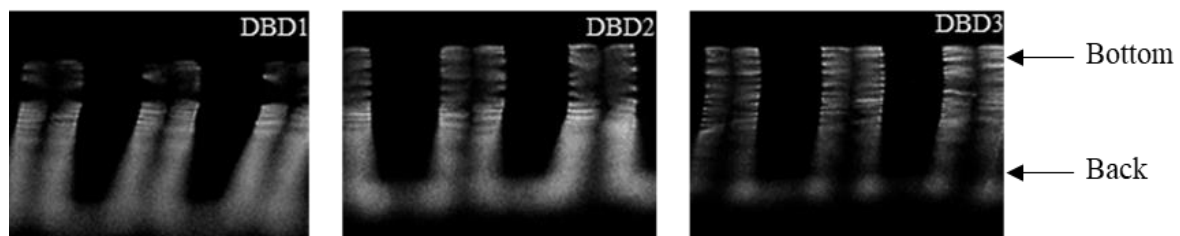

Figure 10. Photographs of the micro discharges along the electrodes and at the bottom of the dielectric barrier.

3.3. Chemical characterization

The reactor exhaust gas was analyzed by FTIR spectroscopy. The absorbance spectrum obtained with an applied voltage of 7.6 kV at 5 kHz is illustrated in Figure 11. Note that a flow of 0.1 L.min^{-1} of reconstituted air at atmospheric pressure was injected as working gas.
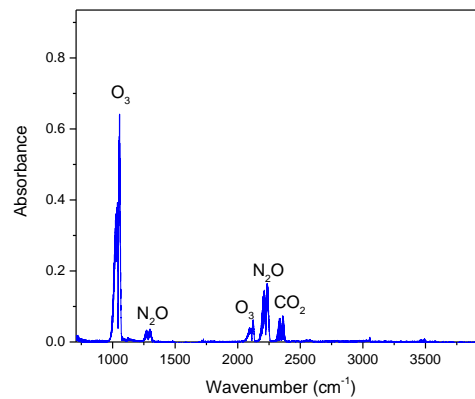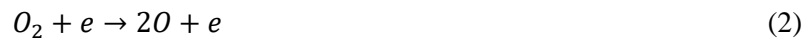

Figure 11. Typical absorbance spectrum of the plasma gas.

Some of the reactions that could result from the interaction of air with the micro discharges, generating species identified in the spectrum, are as follows [12]:

$$O_2 + e \rightarrow 2O + e \qquad (2)$$
$$O + O_2 + M \rightarrow O_3 + M \qquad (3)$$
$$2N_2 + O_2 \rightarrow 2N_2O \qquad (4)$$
$$O + O_3 + M \rightarrow 2O_2 + M \qquad (5)$$

By using reconstituted air, ozone is the essential reactive species generated by the plasma. Figure 12 shows the relation between ozone concentration and dissipated power with the discharge frequency. As explained previously, the dissipated power increases with the frequency. Therefore, more energy is injected in the plasma, so more electrons are produced and participate to the plasma reactions [13]. This phenomenon is on competition with the discharge poisoning effect due to the formation of NO_x molecules, at high power, which completely stops the generation of ozone [14]. To study this phenomenon, the power density was calculated by dividing the power by the area exposed to the plasma (about 7.5 cm^2). The ozone concentration increases from 1.36 g.m^{-3} for a power density of 0.02 W.cm^{-2} at 1 kHz to 2.14 g.m^{-3} for 0.13 W.cm^{-2} at 5 kHz. It keeps increasing with the power density to reach a value of 2.46 g.m^{-3} at 10 kHz. This continues increasing of ozone generation shows that our discharge is working in non-poisoning regime for these experimental conditions. Moreover, by multiplying the concentration by the flow of air and dividing by the power, the obtained value at 1 kHz is equal to 45 g.kW^{-1}.h^{-1}. This value is two times bigger than that obtained in a previous study for a similar configuration [15].
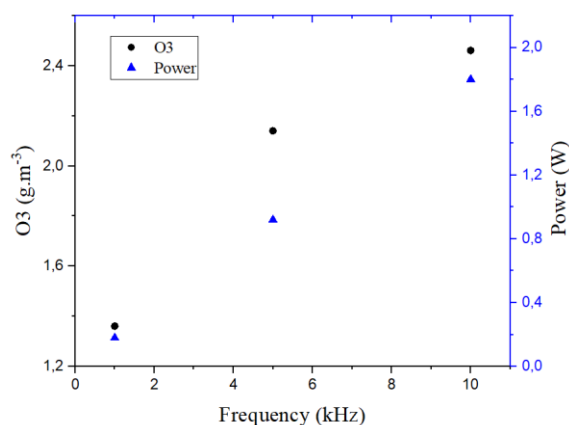
Figure 12. Ozone concentration and dissipated power as function of the discharge frequency.

We must mention that, in this study, we limited the frequency at 10 kHz to avoid the overheating of the dielectric barrier which can lead to the breakdown of the dielectric. In fact, the energy lost in the dielectric is proportional to the frequency of the applied voltage for a given amplitude. Moreover, several studies showed that when the number of reactions increases, the competition between formation of ozone (reaction 3) and its dissociation (reaction 5) becomes rougher which leads to a steady or even decreasing ozone level [7, 12].

Complementary analyses by micro gas chromatography have been done to identify the origin of CO_2 present in FTIR spectrum. This technique has a faster response rate than the FTIR since the volume of analyzed gas is much smaller. We focused on the peak of CO_2 appearing at a retention time of 33 s. The chromatograms were acquired at three different times. Before plasma, when the power supply was turned off. During plasma, with the presence of micro discharges and after plasma when the power supply was turned off again. Reminding that a flux of 0.1 L.min^{-1} of reconstituted air was injected continuously in the reactor. Table 1 shows the concentration of CO_2 present in the plasma exhaust gas at the three times. The presence of CO_2 only when the plasma operates proves that it comes from the interaction of the micro discharges with the dielectric material, since we used reconstituted air (79% N_2, 21% O_2). Thus, carbon atoms should come from the carbon chains of the polymer constituting the dielectric, broken by the micro discharges. We were interested also in the variation of the oxygen peak situated at 48.5 s. It shows a loss of 0.1 % during plasma, corresponding to 1000 ppm of O_2 molecules or 666 ppm (1.42 mg.L^{-1}) of O_3. This concentration is slightly greater than the value measured by FTIR for the same discharge parameters. It could be considered, that O_2 consumed by the micro discharges, was transformed mostly in ozone with little contribution in the formation of N_2O and CO_2.

Table 1. Concentration of CO_2 and O_2 present in the plasma gas.

	CO_2 (%)	O_2 (%)
Before plasma	0	20.95
During plasma	0.004	20.85
After plasma	0	20.95

4. Conclusion

In this work, a compact atmospheric pressure surface dielectric barrier discharge plasma reactor was designed and fabricated with 3D printing. The reactor was designed to be compatible with our SALD head. The aim of the reactor is to assist the SALD process by generating reactive species to the

deposition surface. The geometry of the DBD arrangement was found to be influencing the distribution of the micro discharges on the dielectric surface. Studies were done with three different thicknesses. A variable thickness from 3.4 mm at the beginning of the discharge zone, to 2.2 mm at the bottom showed a homogenous distribution of the discharge filaments all along the electrodes. Electrical characterization showed that the dissipated power increases with the frequency for the three DBDs. However, it shows the opposite behavior with the thickness, when this latter increases from 2.2 to 6.4 mm, the dissipated power decreases from 3.3 to 2 W respectively. Finally, chemical characterization of the plasma gas by FTIR spectroscopy and micro gas chromatography showed the formation of ozone in majority in the exhaust gas. Its concentration could be tuned by controlling the frequency from 1.36 g.m^{-3} at 1 kHz to 2.46 g.m^{-3} at 10 kHz.

5. References

[1] R. W. Johnson, A. Hultqvist, and S. F. Bent, "A brief review of atomic layer deposition: from fundamentals to applications," *Mater. Today*, vol. 17, no. 5, pp. 236–246, Jun. 2014.

[2] S. Franke *et al.*, "Alumina films as gas barrier layers grown by spatial atomic layer deposition with trimethylaluminum and different oxygen sources," *J. Vac. Sci. Technol. Vac. Surf. Films*, vol. 35, no. 1, p. 01B117, Dec. 2016.

[3] D. Muñoz-Rojas and J. MacManus-Driscoll, "Spatial atmospheric atomic layer deposition: a new laboratory and industrial tool for low-cost photovoltaics," *Mater. Horiz.*, vol. 1, no. 3, pp. 314–320, Apr. 2014.

[4] Y. Creyghton, A. Illiberib, A. Mioneb, W. van Boekelb, N. Debernardib, M. Seitzb, F. van den Bruelea, P. Poodtb and F. Roozeboom, "Plasma-Enhanced Atmospheric-Pressure Spatial ALD of Al2O3 and ZrO2," *ECS Trans.*, vol. 75, no. 6, pp. 11–19, Aug. 2016.

[5] F. J. van den Bruele *et al.*, "Atmospheric pressure plasma enhanced spatial ALD of silver," *J. Vac. Sci. Technol. Vac. Surf. Films*, vol. 33, no. 1, p. 01A131, Jan. 2015.

[6] H. B. Profijt, S. E. Potts, M. C. M. van de Sanden, and W. M. M. Kessels, "Plasma-Assisted Atomic Layer Deposition: Basics, Opportunities, and Challenges," *J. Vac. Sci. Technol. Vac. Surf. Films*, vol. 29, no. 5, p. 050801, Aug. 2011.

[7] V. H. Nguyen, J. Resende, C. Jiménez, J. Deschanvres, P. Carroy, D. Muñoz, D. Bellet, and D. Muñoz-Rojas, "Deposition of ZnO based thin films by atmospheric pressure spatial atomic layer deposition for application in solar cells," *J. Renew. Sustain. Energy*, vol. 9, no. 2, p. 021203, Mar. 2017.

[8] D. Muñoz-Rojas, V. H. Nguyen, C. Masse de la Huerta, S. Aghazadehchors, C. Jiménez, and D. Bellet, "Spatial Atomic Layer Deposition (SALD), an emerging tool for energy materials. Application to new-generation photovoltaic devices and transparent conductive materials," *Comptes Rendus Phys.*, vol. 18, no. 7, pp. 391–400, Sep. 2017.

[9] B. Dong, J. M. Bauchire, J. M. Pouvesle, P. Magnier, and D. Hong, "Experimental study of a DBD surface discharge for the active control of subsonic airflow," *J. Phys. Appl. Phys.*, vol. 41, no. 15, p. 155201, 2008.

[10] S. Portugal, S. Roy, and J. Lin, "Functional relationship between material property, applied frequency and ozone generation for surface dielectric barrier discharges in atmospheric air," *Sci. Rep.*, vol. 7, Jul. 2017.

[11] J. Pons, E. Moreau, and G. Touchard, "Asymmetric surface dielectric barrier discharge in air at atmospheric pressure: electrical properties and induced airflow characteristics," *J. Phys. Appl. Phys.*, vol. 38, no. 19, p. 3635, 2005.

[12] J. M. Williamson, D. D. Trump, P. Bletzinger, and B. N. Ganguly, "Comparison of high-voltage ac and pulsed operation of a surface dielectric barrier discharge," *J. Phys. Appl. Phys.*, vol. 39, no. 20, p. 4400, 2006.

[13] A. Ozkan, T. Dufour, A. Bogaerts, and F. Reniers, "How do the barrier thickness and dielectric material influence the filamentary mode and CO 2 conversion in a flowing DBD?," *Plasma Sources Sci. Technol.*, vol. 25, no. 4, p. 045016, 2016.

[14] S. Pekárek, "Non-Thermal Plasma Ozone Generation," *Acta Polytech.*, vol. 43, no. 6, Jan. 2003.

[15] D. Hong, H. Rabat, J. M. Bauchire, and M. B. Chang, "Measurement of Ozone Production in Non-thermal Plasma Actuator Using Surface Dielectric Barrier Discharge," *Plasma Chem. Plasma Process.*, vol. 34, no. 4, pp. 887–897, Jul. 2014.

Acknowledgement